IEEE Photonics Journal
An IEEE Photonics Society Publication

Open Access

Polarization-Insensitive Phase-Transmultiplexing and Multicasting of CSRZ-OOK and 4 × RZ-BPSK to 4 × RZ-QPSK via XPM in a Birefringent PCF

Volume 6, Number 2, April 2014

B. M. Cannon
T. Mahmood
W. Astar
P. Boudra, III
T. Mohsenin
Gary M. Carter

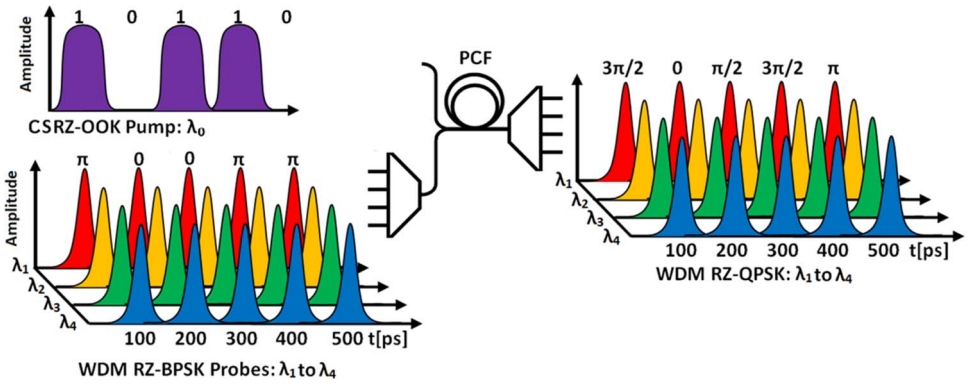

DOI: 10.1109/JPHOT.2014.2309642
1943-0655

IEEE photonics SOCIETY

IEEE

Polarization-Insensitive Phase-Transmultiplexing and Multicasting of CSRZ-OOK and 4 × RZ-BPSK to 4 × RZ-QPSK via XPM in a Birefringent PCF

B. M. Cannon,[1,2,3] T. Mahmood,[1,2,3] W. Astar,[1,3] P. Boudra, III,[2] T. Mohsenin,[2] and Gary M. Carter[1,2,3]

[1]Laboratory for Physical Sciences, College Park, MD 20740 USA
[2]University of Maryland Baltimore County, Baltimore, MD 21250 USA
[3]Center for Advanced Studies in Photonics Research (CASPR), Baltimore, MD 21250 USA

DOI: 10.1109/JPHOT.2014.2309642

Manuscript received January 31, 2014; revised February 26, 2014; accepted February 26, 2014. Date of publication March 4, 2014; date of current version March 24, 2014. Corresponding author: B. M. Cannon (e-mail: cannonb1@lps.umd.edu).

Abstract: By utilizing cross-phase modulation and birefringence, we demonstrated simultaneous polarization-insensitive phase-transmultiplexing and multicasting of a single 10-Gbaud CSRZ-OOK signal and 4 × 10-Gbaud RZ-BPSK signals to generate 4 × 10-Gbaud RZ-QPSK signals in a photonic crystal fiber. The measured receiver sensitivity OSNR penalty at BER of 10^{-9} was ≈1.8 dB, relative to the FPGA-precoded RZ-DQPSK baseline, for a randomly polarized CSRZ-OOK signal, when the launch angles of all RZ-BPSK signals were fixed at ≈45°. In addition, the OSNR of the remotely generated CSRZ-OOK signal could be degraded down to ≈34 dB/0.1 nm, before the BER performance of the phase-transmultiplexing and multicasting operation began to degrade.

Index Terms: Fiber nonlinear optics, fiber optics systems, Kerr effect.

1. Introduction

Many networks are currently being upgraded from on-off-keying (OOK) to the more robust phase-modulated formats, such as binary phase-shift keying (BPSK), due to PSK's improved performance in ASE-limited transmission systems, and tolerance to the various transmission impairments [1]. One of the more common multi-level formats used with differential detection receivers is quadrature (Q)PSK, which is more spectrally efficient than BPSK since the per symbol bit-rate is doubled while the spectral occupancy is nearly the same as that of BPSK. In general, QPSK is less tolerant than BPSK to phase impairments and receiver imperfections, due to a ∼30% reduction in the distance between the constellation vectors in the complex plane [2]. As networks are upgraded, situations can arise where OOK and PSK signals are simultaneously transmitted over DWDM systems, which can lead to PSK signal phase corruption via cross-phase modulation (XPM) induced by the co-propagating OOK signals [3]. In order to avoid this multi-format incompatibility, nonlinear all-optical signal processing (NOSP) has been investigated for traffic grooming and to help maintain network

transparency at network nodes. One such NOSP operation is phase-transmultiplexing (PTM) of OOK and BPSK to QPSK, which has been demonstrated in a passive, highly nonlinear fiber (HNLF), utilizing an OOK pump copolarized with a BPSK probe [4]. The term PTM was coined to describe the NOSP operation of transferring and multiplexing the data of an OOK pump with the phase data of a BPSK signal to generate a QPSK signal, utilizing XPM. The resultant QPSK signal was composed of in-phase (I) and quadrature (Q) components, which carried the data of the original BPSK and OOK channels, while occupying the same spectral slot as the BPSK signal. However, for the PTM operation to be more viable in realistic systems where the states-of-polarization (SOP) of the signal can continuously change, it is important to mitigate the polarization dependence of the underlying Kerr nonlinearities. A commonly used method to enable polarization-insensitive (PI) NOSP in pump-probe experiments, exploits the deterministic birefringence in a nonlinear device by adjusting the launch angle of the pump/probe to reduce the per-axis nonlinearity fluctuations [5]. In addition to launch angle adjustment, a device-dependent minimum pump-probe detuning (PPD) is also required to further reduce fluctuations [6]. The first demonstration of PI-PTM was in a passive AlGaAs waveguide using the polarization sensitivity reduction method outlined in [6], [7] and was essentially a proof-of principle demonstration [8]. The damage threshold of the AlGaAs waveguides in [8] prevented the use of more realistic pulse-widths to maintain the required intensity needed for the nonlinear phase shift. In principal this can be overcome by engineering longer waveguides with lower propagation loss and better mode adapters to reduce the coupling loss of 3 dB/facet [8]. However, this would require significantly more materials development. Photonic crystal fiber (PCF) is a good candidate for PTM with realistic pulse-widths since it has a low propagation loss of 0.008 dB/m, a relatively large nonlinear coefficient of $\approx 11\ \mathrm{W \cdot km^{-1}}$. In addition, the PCF used in [5] has been found to exhibit a large group-index birefringence on the order of $10^{-5} - 10^{-4}$, and a dispersion slope of $\approx 10^{-2}\ \mathrm{ps \cdot nm^{-2} \cdot km^{-1}}$, which allows PI-NOSP to be carried out in the PCF using the same polarization sensitivity reduction technique as in the AlGaAs waveguide, but without the added complexity of short pulse generation. Although HNLF would allow a large enough input optical power $>$ 30 dBm to achieve PTM, its birefringence is insufficient to enable polarization-insensitive operation using the same method. Depending on network architecture and system requirements, simultaneous PTM and multicasting (PTMM) could be used to broadcast remotely generated data over pre-configured BPSK channels slots at network optical add-drop cross-connects, while maintaining transmission compatibility with other PSK channels. Therefore, this report is focused on the first demonstration of simultaneous PI-PTMM via XPM in a 30-m nonlinear birefringent PCF, of a CSRZ-OOK pump and 4 $\times$ RZ-BPSK probes, with realistic duty-cycles of 66.7% and 33.3%. To emulate ASE-limited transmission, the OSNR of the CSRZ-OOK signal was degraded and the performance of the resultant RZ-QPSK signals were evaluated with conventional ASE-loaded receiver sensitivity measurements.

2. Principle of Operation

The proposed PTMM to 4 $\times$ 10-Gbaud RZ-QPSK via XPM is shown in Fig. 1, where the probes are 4 $\times$ 10-Gbaud RZ-BPSK and the pump is a single 10-Gbaud CSRZ-OOK signal. In the process, the CSRZ-OOK pump data is multi-cast via XPM to the 4 $\times$ RZ-BPSK signals, which are consequently converted to 4 $\times$ RZ-QPSK signals at the output of the PCF. The idealized phase of the jth probe after propagation in the PCF, whose physical length is much smaller than the smallest dispersion length for the signals considered, and considering only copolarized XPM and self-phase modulation (SPM), is described by

$$\begin{aligned}\phi_{j\,out}(t) &\approx \phi_{j,\,in}(t) + \phi_{j\,\mathrm{SPM}}(t) + \phi_{0\mathrm{XPM}}(t) + \sum_{m=1}^{M}(1-\delta_{mj})\phi_{m\mathrm{XPM}}(t) \\ &\approx \phi_{j\,in}(t) + \gamma L_{\mathrm{eff}} P_j(t) + 2\gamma L_{\mathrm{eff}} P_0(t) + 2\gamma L_{\mathrm{eff}} \sum_{m=1}^{M}(1-\delta_{mj})P_m(t). \qquad (1)\end{aligned}$$

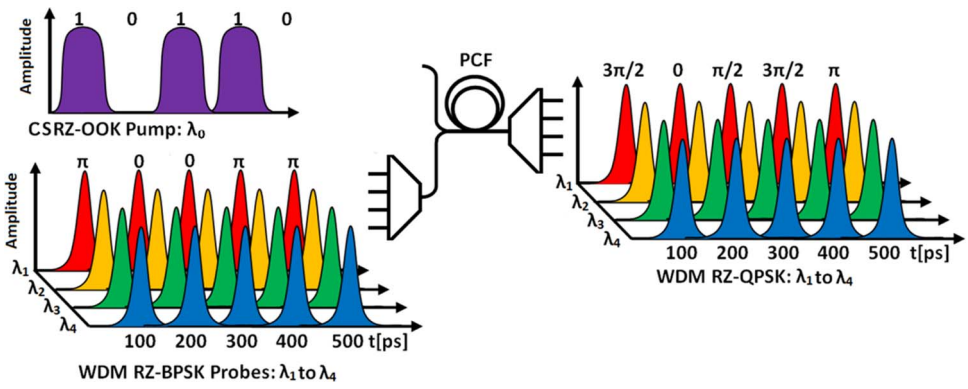

Fig. 1. Scheme for PTMM to 4 × RZ-QPSK using a 4 × RZ-BPSK probe and a single CSRZ-OOK pump.

The nonlinear coefficient and effective length for a single SOP are represented by γ and L_{eff}, respectively. The peak power of the mth channel is P_m, and M is the total number of WDM probe channels. The XPM phase from the pump is represented by $\phi_{0\text{XPM}}$ and P_0 is the peak power of the pump. From Eq. (1) it is clear that the effective phases of the probes are time-dependent function of their respective input phases, as well as pump-induced XPM and probe-induced SPM and XPM. The bit-wise probe-induced SPM and XPM phase shifts are periodically identical with the probe power due to the constant power envelope of the probes. Consequently, the phase shifts due to the probes are eliminated in a differential detection receiver that includes a 1-bit-delay asymmetric Mach–Zehnder interferometer (AMZI). In addition, the pulse-width of the pump should be sufficiently large to ensure a nearly uniform XPM phase shift over the duration of the probe pulses during the occurrence of a ONE-bit in the pump, to minimize chirp [6], [9], [10].

Since the PTMM operation requires a high-power pump and several probes to be launched into the PCF, it is especially important to allocate the channels appropriately on the ITU grid, so that inter-channel cross-talk due to FWM is minimized. In addition, the 30-m PCF used in the PTMM experiment had a nearly flat dispersion profile, with a dispersion coefficient (D) $\approx$0.6 ps$\cdot$ nm^{-1} $\cdot$ km^{-1} at 1550 nm and a dispersion slope (S) $\approx$0.0122 ps $\cdot$ nm^{-2} $\cdot$ km^{-1}. For the power used in the PTMM operation, the first-order FWM terms are unacceptably efficient over the entire C-Band. Consequently, the probe channels are chosen so that no first-order partially-degenerate, or non-degenerate FWM terms overlap with either a pump or a probe channel. Furthermore, the probe powers must be sufficiently low to prevent degradations due to second-order FWM. Given the input channel slot number, represented by i, j, k, the output channel slots occupied by FWM terms are given by [11]

$$n_{ijk} = n_i + n_j - n_k; \quad (k \neq i, j). \tag{2}$$

For any choice of i, j, k on an ITU-standardized channel grid, the generated FWM term should not coincide with an occupied pump or probe channel slot. Using Eq. (2), and assuming all FWM terms are significant, the probe channels must utilize an unequal channel spacing scheme to minimize inter-channel FWM crosstalk [11], [12]. Although inter-channel crosstalk due to FWM can be minimized using the unequal channel spacing technique, optical parametric amplification (OPA) of the probes via FWM cannot be minimized as easily [13]. In addition, OPA can be significantly degrading to the PTMM operation, which will be discussed later in this report. To enable polarization-insensitive operation in the PCF, all of the probes are launched off-axis at approximately 45° between the birefringent axis of the PCF to equalize the per-axis XPM phase shift [7]. In addition to the launch angle adjustment, a minimum PPD is required to further minimize polarization-induced fluctuations, which takes the following form [6], [14]

$$\Delta\lambda_{DGD} = \frac{a\lambda_0^2}{c \cdot DGD}; \quad a \in Z^+. \tag{3}$$

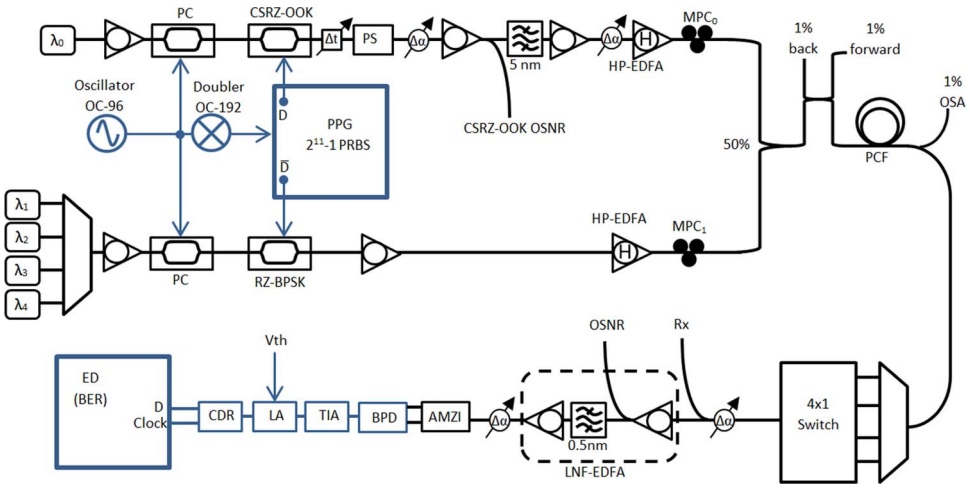

Fig. 2. Experimental setup for PTMM to QPSK. (PPG: pulse pattern generator, Δt: optical delay line, PRBS: pseudo-random bit-sequence, PC: pulse carver, MPC: mechanical polarization controller, $\Delta\alpha$: variable optical attenuator, PS: polarization scrambler, HP-EDFA: high power erbium-doped fiber amplifier, LNF-EDFA: low-noise-figure EDFA, AMZI: asymmetric Mach–Zehnder interferometer, BPD: balanced photo-detector, TIA: transimpedance amplifier, LA: limiting amplifier, V_{th}: threshold voltage, CDR: clock-data recovery module, ED: error-detector, OSA: optical spectrum analyzer), P_{Rx}: received power.

The magnitude of the PCFs' differential group delay is represented by *DGD*, *c* is the speed of light, and λ_0 is the pump wavelength.

3. Experimental Results and Discussion

3.1. Experimental Setup

The experimental setup for PTMM to 4 $\times$ 10-Gbaud RZ-QPSK via XPM is shown in Fig. 2. The 4 probes were 10-Gbaud RZ-BSPK $2^{11}-1$ pseudo-random bit sequences (PRBS), centered at 1546.1 nm, 1545.3 nm, 1543.7 nm, and 1540.5 nm, each with a pulse-width of $\approx$33. 3 ps. The 10-Gbaud CSRZ-OOK pump, which served as the remotely generated signal in the experiment, was also $2^{11}-1$ PRBS and centered at 1559.7 nm with a pulse-width of $\approx$66.7 ps. The PPD was chosen to be larger than the previously reported 6 nm minimum PPD required to reduce polarization fluctuations, and to enable PI operation in a 30-m PCF [6].The minimum required PPD was also verified experimentally, using Eq. (3) in conjunction with the Rashleigh DOP method as outlined in [14], [15], to be approximately 6.3 nm. In addition to the minimum PPD requirement, the pump also needs to be detuned from the probes to minimize inter-channel cross-talk due to FWM. The 30-m PCF also exhibited a propagation loss of approximately 0.008 dB/m, a nonlinear coefficient of $\approx$11 $W \cdot km^{-1}$ and a dispersion coefficient with a wavelength (λ) dependence as $D(\lambda) \approx (S \cdot \lambda - 19.5)$ $ps \cdot nm^{-1} \cdot km^{-1}$, where λ has units of nm. The pulse-widths of the pump and the probes were chosen to ensure near-uniform XPM over the duration of the probe pulse during the occurrence of a one-bit in the pump, thus minimizing chirp. The pump pulse-width was chosen to be the maximum standard pulse-width, which allowed the desired XPM phase shift to be obtained with minimal stimulated Brillouin scattering (SBS), as discussed in the next section. The pump and the probes were separately amplified in high-power (HP) erbium-doped fiber amplifiers (EDFA), and temporally synchronized using an optical delay line. The SOPs for all signals were separately adjusted using mechanical polarization controllers just after their respective HP-EDFAs. In order to emulate ASE-limited transmission, the pump OSNR was varied before its HP-EDFA, and the SOP of the signal was randomized using a polarization scrambler. The signals were subsequently combined using a 50% fused-silica-fiber coupler, followed with a 2 $\times$ 2 1%-diagnostic tap, and launched into the

PCF. For all the SOPs considered, the average pump power illuminating the PCFs' input mode adapter was ≈29.3 dBm, which was the optimum power required to induce a XPM $\pi/2$ phase shift on the RZ-BPSK probes when the pump SOP was randomized, and the probes were all launched off-axis at ≈45°. The per-channel RZ-BPSK probe powers were chosen to be ≈15 dBm, in order to maintain sufficient OSNR at the output of the PCF, while simultaneously avoiding excessive second-order FWM cross-talk. The resultant PTMM 4 × RZ-QPSK signals, which were previously the 4 × RZ-BPSK probes, were subsequently isolated at the output of the PCF using a 100-GHz channel-spaced arrayed waveguide grating with a Gaussian passband −3-dB bandwidth of 0.45 nm. The PTMM RZ-QPSK signals were subsequently analyzed individually as DQPSK signals using a differential-detection receiver. The DQPSK receiver consisted of a dual-stage, high-gain low-noise-figure (LNF) EDFA with an inter-stage Gaussian filter, with a −3-dB bandwidth of 0.5 nm for the elimination of out-of-band ASE that could compete with the signal for the gain of the second amplification stage. The remainder of the 10-Gbaud receiver consisted of a 1-bit-delay AMZI, a balanced photo-detector, a transimpedance amplifier, a limiting amplifier (LA), followed by a standard 10-Gbaud clock-data recovery module, and an error detector (ED). The bit-error ratio (BER) threshold was set by the LA and the optimal threshold was approximately the same for all signals. For DQPSK receiver sensitivity measurements, a variable optical attenuator (VOA) was placed just before the LNF EDFA to vary the received power, while the average optical power incident on each detector of the BPD was held constant at ≈ −1 dBm by a second VOA just before the AMZI. The *I* and *Q* components of the RZ-QPSK signal were analyzed separately by adjusting the AMZI bias to ≈ $\pm\pi/4$ and error detection of the PTMM RZ-QPSK signals was made possible by uploading the AMZI output (found from a simulation) to the ED. The baseline RZ-DQPSK signal was precoded at the transmitter using a Xilinx Virtex 6 FPGA and modulated onto the optical carrier at 1546.1 nm using a conventional $LiNbO_3$ nested IQ-modulator so that the detected signal after the AMZI was $2^{11} - 1$ PRBS, as described in [8]. The pulse-width of the RZ-QPSK baseline signal was identical to the probe's in the PTMM experiment, to ensure identical receiver responses [16].

3.2. Stimulated Brillouin Scattering Threshold Characterization

The initial SBS threshold characterization was carried out by recording the average back-reflected power from the PCF as a function of average input power. The backward propagating power was measured using a power monitor on the reverse port of the 2 × 2 1%-diagnostic tap just before the PCF in Fig. 2, which measured the sum of all reflections, as well as the SBS backward-propagating power. The forward propagating signal power was measured using the forward 1%-port and a polarization analyzer, which served the dual purpose of SOP verification and power monitoring. The starting point for the measurements was the highest available power into the PCF mode adapter, limited by the EDFA, so that the single-axis launch condition could be identified by maximizing the variance of the one-rail due to SBS in the eye-diagram, after having passed through the receiver in Fig. 2. The eye-diagram was observed with a 40-GHz PD into a 50-GHz sampling module, Fig. 3(a) [17]. The single-axis SOP was subsequently recorded on the polarization analyzer and the launch power was gradually lowered, while ensuring the SOP was adjusted after each power transition to correct for any polarization drift. The 45° launch condition was reached in a similar manner, except it was identified by minimizing the variance of the one rail, as shown in Fig. 3(b) [17]. The measurement was subsequently carried out for a NRZ-OOK signal and a CSRZ-OOK signal centered at 1559.7 nm, each for the single-axis and 45° launch conditions, Fig. 4(a).

The NRZ-OOK signals' SBS threshold for the single-axis condition was determined to be ≈27 dBm into the PCF mode adapter, and ≈30 dBm for the 45° launch condition, which was several dB below the power required for an XPM-induced $\pi/2$ phase shift. The additional 3 dB improvement for the 45° launch condition was due to the total power being split between the two birefringent axes. As expected, the CSRZ-OOK signals' SBS threshold showed a significant improvement over the NRZ-OOK signal due to a larger bandwidth [18], with the threshold being extended to ≈31 dBm for the single-axis condition. Due to insufficiently powerful HP-EDFAs, the SBS threshold was not observed when the CSRZ-OOK signal was launched off-axis, which located the threshold at > 33 dBm.

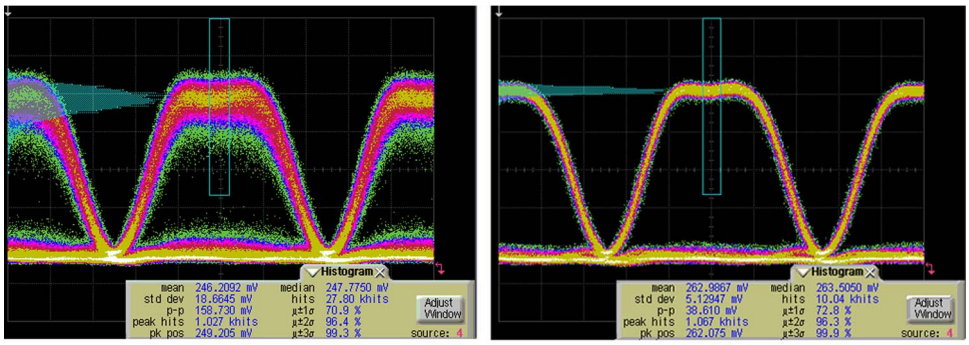

(a) (b)

Fig. 3. CSRZ-OOK pump eye-diagrams for an average input power into the PCF mode adapter of approximately 31.6 dBm, captured in ≈20-second color-grade infinite persistence mode using a 40-GHz detector into a 50-GHz sampling module. The SOP of the signal was (a) launched along a single-axis, and (b) launched at 45°.

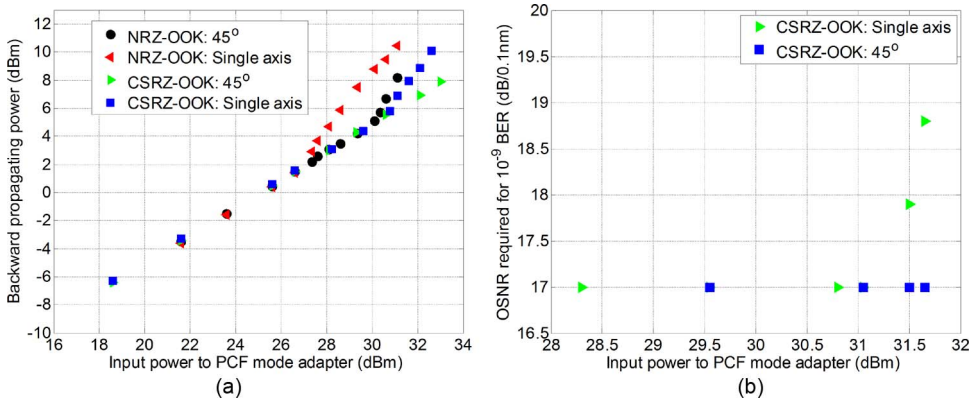

(a) (b)

Fig. 4. SBS threshold characterization (a) backward-propagating power as a function of input power into the PCF mode adapter. (b) Minimum OSNR to reach a BER metric of 10^{-9} for CSRZ-OOK only as a function of input power to the PCF mode adapter.

Receiver sensitivity measurement was subsequently carried out on the CSRZ-OOK signal for the various input power levels to determine BER performance below and above the SBS threshold, in Fig. 4(b). Below the SBS threshold there was no penalty, within experimental error, associated with increasing the signal power, but above the SBS threshold of 31 dBm the OSNR penalty rapidly increased. In addition, the SBS backward-propagating power measurements showed strong correlation with the more quantitative receiver sensitive measurement and the PTMM operating point of ≈29.3 dBm for the pump was determined to be adequately below the SBS threshold to avoid an unnecessary BER penalty.

3.3. Demonstration of PTMM and OPA

As mentioned before the PCF has a nearly flat dispersion profile and low dispersion across the entire C-band, consequently OPA was present across the entire C-band. In order to qualitatively examine the effect of OPA only, the probe at 1546.1 nm and the pump were propagated in the PCF, with the total power of the pump and probe being the same as in the PTMM experiment. The probe closest to the pump was used because it was expected to be the worst case scenario, since the OPA and FWM were fractionally more efficient, due to the smaller phase-mismatch of the pump and probe [13]. The probe was subsequently isolated at the output of the PCF and detected using a

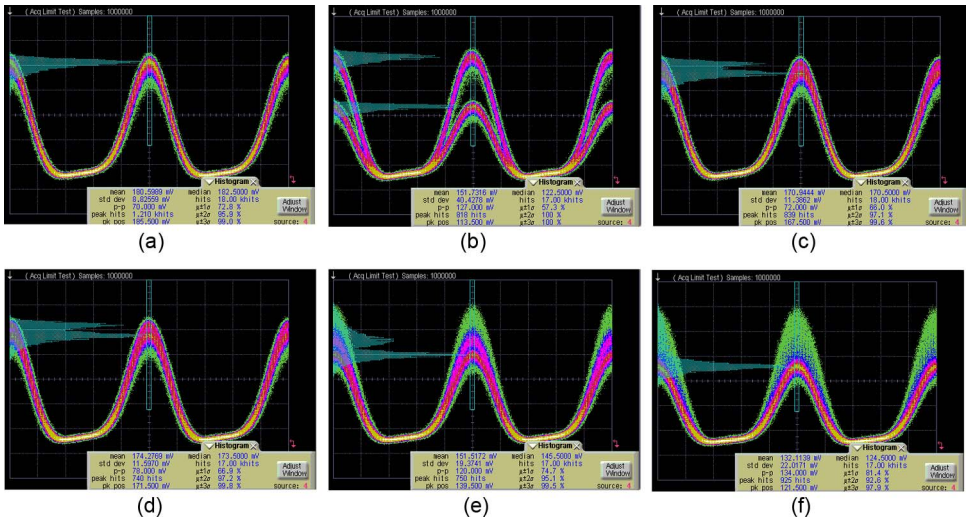

Fig. 5. Eye-diagrams of RZ-QPSK signal before the AMZI at an OSNR > 35 dB / 0.1 nm, captured in ≈20-second color-grade infinite persistence mode using a 40-GHz detector into a sampling module with a 50-GHz bandwidth. Eye-diagrams before the receiver AMZI, when the: (a) pump is off and probe is launched along a single-axis, and the PTM RZ-QPSK signal when the: (b) pump || probe || single axis, (c) probe perpendicular to pump || single-axis, (d) pump || single-axis and probe launched off axis at approximately 45°, (e) pump polarization-scrambled and probe launched off-axis at approximately 45°, and (f) pump polarization-scrambled and probe || single-axis.

50-GHz PD into a 40-GHz sampling module. The eye-diagram in Fig. 5(a) is the RZ-BPSK probe, captured just before the AMZI, when the pump was deactivated and the probe was launched along a single-axis in the PCF. All subsequent eye-diagrams in Fig. 5 are for the PTMM operation under various SOP conditions with the input pump and probe OSNRs > 45 dB/0.1 nm. The case of the pump co-polarized with the probe along a PCF birefringent axis, was obtained by maximizing the generated FWM idler at the output of the PCF, and subsequently optimizing OPA of the probe. The resultant signal shows significant OPA for every occurrence of a ONE in the pump, and no OPA for every ZERO, which leads to the formation of two distinct rails in the eye-diagram, Fig. 5(b). In order to eliminate OPA, the pump could be launched perpendicular to the probe as in Fig. 5(c), but this leads to an insufficient XPM-induced phase shift. In order to minimize OPA, while maintaining sufficient XPM on the probe, it was discovered that the pump should be launched along a single-axis and the probe should be launched between the axes at approximately 45°, Fig. 5(d). This was expected to be the "best" stationary SOP condition for the PTMM operation instead of pump and probe aligned to a single-axis. If the pump polarization scrambler were activated, while the probe was launched at 45°, OPA and XPM fluctuations would be minimized, as in Fig. 5(e). Alternatively if the probe was launched along a single-axis, while the pump SOP was randomized, the OPA and XPM fluctuations were maximized, as shown by the increase in the eye-diagrams' standard deviation, Fig. 5(f). Therefore, based on the observations of OPA and previous knowledge of the requirements for polarization-insensitive operation, the optimal conditions for polarization-insensitive operation were for the probe to be launched at 45°, while the pump SOP was randomized. Consequently, only the two "best"-case scenarios were analyzed with receiver sensitivity measurements for the PTMM operation. The FPGA precoded baseline eye-diagrams after the AMZI, Fig. 6(a), were qualitatively similar to the optimized stationary SOP condition of the pump aligned to a single-axis with the probes launched at 45° for the *I* and *Q* components, Fig. 6(b). In addition, an average 10^{-9}-BER pre-amplified receiver sensitivity penalty of only ≈0.8 dB was demonstrated relative to the FPGA precoded baseline RZ-DQPSK, Fig. 7(a). Much of the penalty is due to residual OPA, receiver electronic response variation, experimental error, and chirp. The penalty for this case and all subsequent cases is the average of the *I* and the *Q* signals for all 4 channels and quoted relative to the FPGA precoded baseline. The optimized polarization-insensitive case of pump scrambled and probes launched at 45° demonstrated

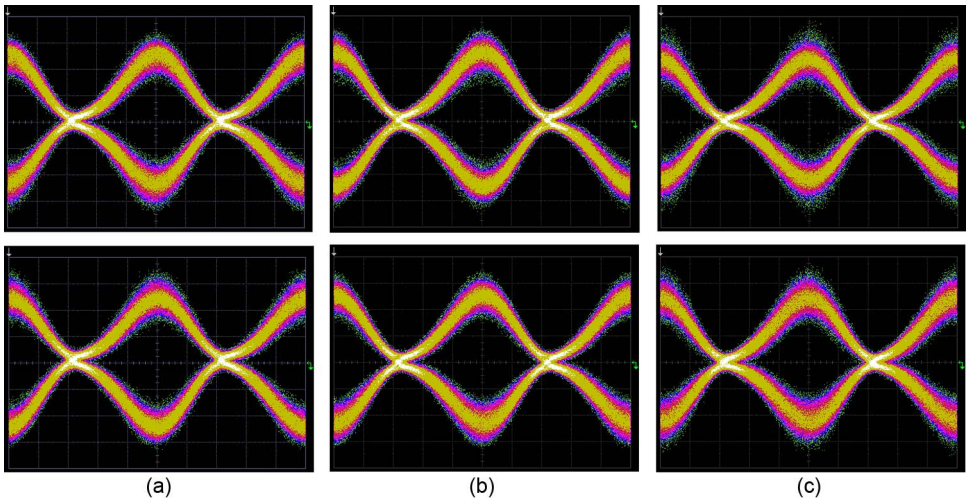

Fig. 6. Eye-diagrams of RZ-(D)QPSK signal after the AMZI at an OSNR > 35 dB / 0.1 nm, captured in ≈20-second color-grade infinite persistence mode using a 40-GHz detector and a 12 GHz TIA, into a 40-GHz sampling module. For the a) baseline *I* (top) and *Q* (bottom) and for the PTMM operation for the: (b) pump ‖ single-axis with the probe launched at 45°, (c) pump polarization scrambled with the probe launched at 45°.

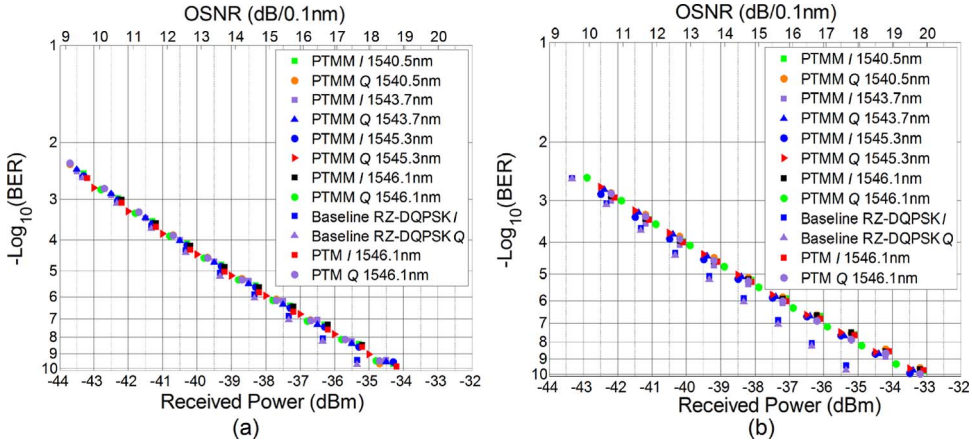

Fig. 7. Receiver sensitivity measurements for PTMM RZ-QPSK when (a) pump aligned to a single-axis and the probe launched at 45°, and (b) pump SOP scrambled and the probe launched at 45°. Baseline RZ-DQPSK was precoded using a Virtex 6 FPGA and modulated onto an optical carrier with a conventional $LiNbO_3$ nested IQ-modulator.

an eye-diagram with increased rail variance relative to RZ-DQPSK baseline, Fig. 6(c), and a penalty of only ≈1.8 dB, Fig. 7(b). The penalty is believed to be caused by fluctuations in OPA efficiency due to the randomized pump SOP and residual XPM fluctuations due to experimental error in launch angle adjustment. In order to compare the PTMM penalty to the single channel PTM operation, the 3 probes farthest from the pump were deactivated. The resultant signal performed approximately the same as the PTMM to QPSK for both polarization conditions considered, which demonstrates nearly no additional penalty associated with the multi-channel PTMM operation when proper steps were taken to minimize FWM-induced inter-channel crosstalk and OPA. The OSNR penalty for the pump aligned to a single-axis with the probe launched at 45° was within experimental error at a BER metric of 10^{-4}, when ASE became the dominant corrupting mechanism. Furthermore, the PI-PTMM operation demonstrated a greatly reduced penalty of only ≈0.5 dB at 10^{-4}-BER. The 10^{-4}-BER metric was

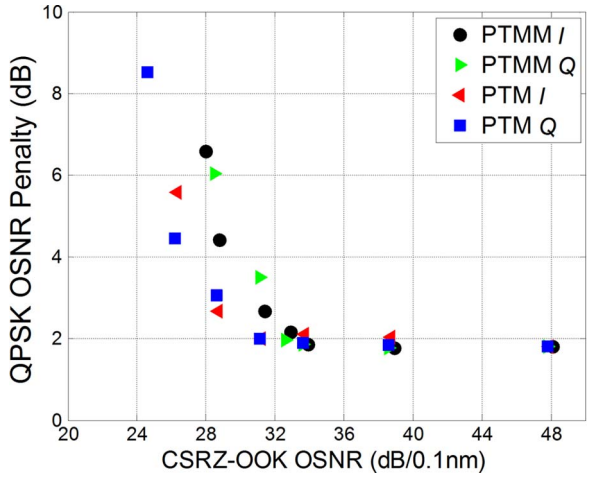

Fig. 8. QPSK *I*- and *Q*- OSNR penalty at 10^{-9} BER relative to the FPGA pre-coded baseline as a function of CSRZ-OOK OSNR for the PTMM operation (the DWDM-probe case) and the PTM operation (the single-channel probe case).

considered assuming the possibility of implementing the *ITU*-T G.709 standard RS(255,239) forward-error correction with ≈7%-over-head, which can correct an un-coded BER of up to $\approx 10^{-4}$ to a BER close to 10^{-13}. However, for this consideration, the single-carrier net information rate of 10-Gbaud is reduced by ≈7%.

3.4. OSNR Degradation Investigation

The previously discussed PTMM operation was carried out as a proof of principle with an input CSRZ-OOK OSNR > 45 dB/0.1 nm, which was the unrealistic case and not representative of a practical system. Consequently, ASE-limited transmission of the CSRZ-OOK pump was emulated by degrading its OSNR, and the impact of OSNR degradations was quantified with receiver sensitivity measurements. The CSRZ-OOK pump signal was noise-loaded by attenuating the signal using a VOA and passing it through an EDFA, just before its respective HP-EDFA. The OSNR was measured just after the EDFA using an optical spectrum analyzer, while the average power into the HP-EDFA was held constant using a second VOA, Fig. 2. The OSNR of the 4 RZ-BPSK signals remained > 45 dB/0.1 nm since the signals are considered to be locally generated. The input CSRZ-OOK power into the PCF was fixed at the optimal value required for the $\pi/2$ phase shift. The required probe OSNR to reach a BER metric of 10^{-9} for the RZ- DQPSK signal was subsequently recorded for the several different CSRZ-OOK OSNR points, for the probe with the smallest PPD. The OSNR penalties relative to QPSK baseline are summarized in Fig. 8. Only the smallest PPD was measured since it was considered the worst-case scenario, previously discussed in Section 3.3. It was found that the OSNR of the CSRZ-OOK pump signal could drop to ≈34 dB/0.1 nm before any significant penalty was observed, and after this point the OSNR penalty increased dramatically with decreasing CSRZ-OOK OSNR. It may be noted that the *I*- and *Q*-components performed differently at lower CSRZ-OOK OSNR, but this is attributed to experimental error. In order to have a point of comparison for the PTMM (the DWDM-probe case) operation, the 3 probes with the larger PPD were deactivated and the measurement was repeated for the PTM (the single-channel probe case) operation. As shown in Fig. 8 the PTM operation has an additional ≈3 dB tolerance to CSRZ-OOK degradations. It was discovered that the PTMM operation was more susceptible to CSRZ-OOK OSNR degradations due to the transfer of the noise pedestal around the CSRZ-OOK to the probes via FWM. The progression of the noise pedestal induced on the probe(s) is shown in the power spectra captured for the PTM and PTMM operations and several different CSRZ-OOK pump OSNRs, Fig. 9. As the CSRZ-OOK signal's OSNR was degraded, for the PTM operation, the noise pedestal became increasingly significant and effectively noise-loaded the probe, Fig. 9(a). For the PTMM operation, the

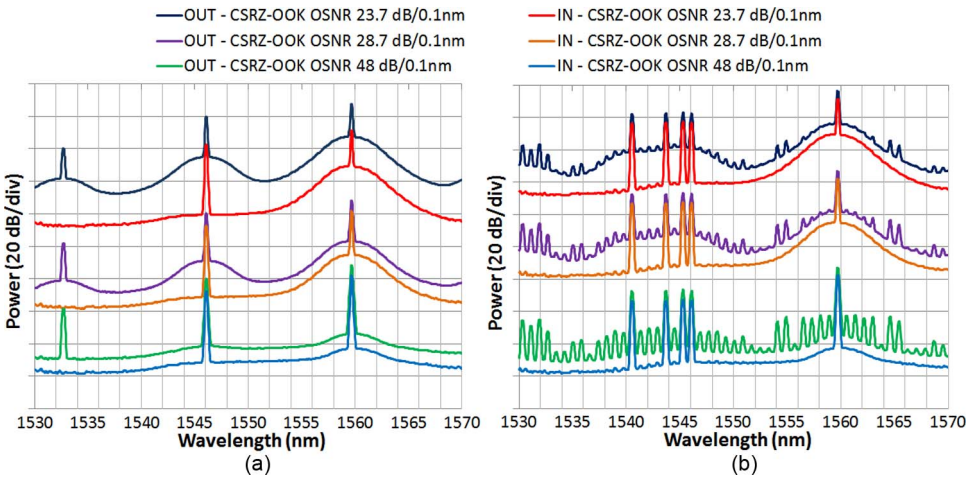

Fig. 9. Power spectra for various CSRZ-OOK OSNRs, captured at a resolution bandwidth of 0.06 nm for the (a) PTM operation and (b) PTMM operation.

FWM-induced noise pedestal expanded to neighboring probe channels resulting in additional noise, which was not observed for the PTM operation, Fig. 9(b).

4. Summary and Conclusion

The PI-PTMM operation was successfully demonstrated in a 30-m-long PCF with a 10^{-9}-BER receiver sensitivity penalty of ≈1.8 dB relative to the FPGA-precoded RZ-QPSK baseline. At a BER metric of 10^{-4} the penalty for the PI-PTM to RZ-DQPSK was reduced to only ≈0.5 dB, relative to baseline RZ-DQPSK. It was also shown that the PI-PTMM operation could tolerate a CSRZ-OOK pump OSNR degradation to only ≈34 dB/0.1 nm before the PI-PTMM QPSK OSNR required to reach 10^{-9}-BER began to rapidly increase.

References

[1] G. Raybon, A. Adamiecki, P. J. Winzer, S. Randel, L. Salamanca, A. Konczykowska, F. Jorge, J.-Y. Dupuy, L. L. Buhl, S. Chandrashekhar, C. Xie, S. Draving, M. Grove, K. Rush, and R. Urbanke, "High symbol rate coherent optical transmission systems: 80 and 107 Gbaud," *J. Lightw. Technol.*, vol. 32, no. 4, pp. 824–831, Feb. 2014.

[2] G. Raybon, A. Adamiecki, P. P. J. Winzer, M. Montoliu, S. Randel, A. Umbach, M. Margraf, J. Stephan, S. Draving, M. Grove, and K. Rush, "All-ETDM 107-Gbaud PDM-16QAM (856-Gb/s) transmitter and coherent receiver," in *Proc. 39th Eur. Conf. ECOC*, 2013, pp. 1–3.

[3] G. Raybon, A. L. Adamiecki, P. Winzer, C. Xie, A. Konczykowska, F. Jorge, J.-Y. Dupuy, L. L. Buhl, S. Chandrashekhar, S. Draving, M. Grove, and K. Rush, "Single-carrier 400G interface and 10-channel WDM transmission over 4,800 km using all-ETDM 107-Gbaud PDM-QPSK," in *IEEE Photon. Technol. Lett.*, 2013, pp. 1–4.

[4] M. Galili, C. Schmidt-Langhorst, R. Ludwig, F. Futami, S. Watanabe, and C. Schubert, "All-optical combination of DPSK and OOK to 160 Gbit/s DQPSK data signals," in *Proc. Conf. Opt. Fiber Commun. Nat. Fiber Opt. Eng. Conf.*, Anaheim, CA, USA, 2007, pp. 1–3.

[5] A. S. Lenihan, R. Salem, T. E. Murphy, and G. M. Carter, "All-optical 80-gb/s time-division demultiplexing using polarization-insensitive cross-phase modulation in photonic crystal fiber," *IEEE Photon. Technol. Lett.*, vol. 18, no. 12, pp. 1329–1331, Jun. 2006.

[6] W. Astar, C.-C. Wei, Y.-J. Chen, J. Chen, and G. M. Carter, "Polarization-insensitive, 40 Gb/s wavelength and RZ-OOK-to-RZ-BPSK modulation format conversion by XPM in a highly nonlinear PCF," *Opt. Exp.*, vol. 16, no. 16, pp. 12 039–12 049, Aug. 2008.

[7] R. Salem, A. S. Lenihan, G. M. Carter, and T. E. Murphy, "Techniques for polarization-independent cross-phase modulation in nonlinear birefringent fibers," *IEEE J. Sel. Topics Quantum Electron.*, vol. 14, no. 3, pp. 540–550, May/Jun. 2008.

[8] B. M. Cannon, T. Mahmood, W. Astar, P. Apiratikul, G. Porkolab, P. Boudra, T. Mohsenin, C. J. K. Richardson, and G. M. Carter, "All-optical amplitude-phase transmultiplexing of RZ-OOK and RZ-BPSK to RZ-QPSK by polarization-insensitive XPM using a nonlinear birefringent AlGaAs waveguide," *Opt. Exp.*, vol. 21, no. 17, pp. 19 885–19 899, Aug. 2013.

[9] K. Mishina, S. Kitagawa, and A. Maruta, "All-optical modulation format conversion from on-off-keying to multiple-level phase-shift-keying based on nonlinearity in optical fiber," *Opt. Exp.*, vol. 15, no. 13, pp. 8444–8453, Jun. 2007.

[10] C. C. Wei, W. Astar, J. Chen, Y. J. Chen, and G. M. Carter, "Theoretical investigation of polarization insensitive data format conversion of RZ-OOK to RZ-BPSK in a nonlinear birefringent fiber," *Opt. Exp.*, vol. 17, no. 6, pp. 4306–4316, Mar. 2009.
[11] F. Forghieri, R. W. Tkach, A. R. Chraplyvy, and D. Marcuse, "Reduction of four-wave mixing crosstalk in WDM systems using unequally spaced channels," *IEEE Photon. Technol. Lett.*, vol. 6, no. 6, pp. 754–756, Jun. 1994.
[12] A. Bogoni and L. Poti, "Effective channel allocation to reduce inband FWM crosstalk in DWDM transmission systems," *IEEE J. Sel. Topics Quantum Electron.*, vol. 10, no. 2, pp. 387–392, Mar./Apr. 2004.
[13] J. Hansryd, P. A. Andrekson, M. Westlund, J. Li, and P. Hedekvist, "Fiber-based optical parametric amplifiers and their applications," *IEEE J. Sel. Topics Quantum Electron.*, vol. 8, no. 3, pp. 506–520, May/Jun. 2002.
[14] B. M. Cannon, W. Astar, T. Mahmood, P. Apiratikul, G. A. Porkolab, C. J. K. Richardson, and G. M. Carter, "Data transfer from RZ-OOK to RZ-BPSK by polarization-insensitive XPM in a passive birefringent nonlinear AlGaAs waveguide," *J. Lightw. Technol.*, vol. 31, no. 6, pp. 952–966, Mar. 2013.
[15] S. Rashleigh, "Origins and control of polarization effects in single-mode fibers," *J. Lightw. Technol.*, vol. 1, no. 2, pp. 312–331, Jun. 1983.
[16] P. J. Winzer and A. Kalmar, "Sensitivity enhancement of optical receivers by impulsive coding," *J. Lightw. Technol.*, vol. 17, no. 2, pp. 171–177, Feb. 1999.
[17] J. E. McElhenny, R. Pattnaik, and J. Toulouse, "Polarization dependence of stimulated Brillouin scattering in small-core photonic crystal fibers," *J. Opt. Soc. Amer. B, Opt. Phys.*, vol. 25, no. 12, pp. 2107–2115, Dec. 2008.
[18] D. A. Fishman and J. A. Nagel, "Degradations due to stimulated Brillouin scattering in multigigabit intensity-modulated fiber-optic systems," *J. Lightw. Technol.*, vol. 11, no. 11, pp. 1721–1728, Nov. 1993.